A Simultaneous Differential Scanning Calorimetry – X-Ray Diffraction Study of Olanzapine Crystallisation from Amorphous Solid Dispersions

Sean Askin,[†] Andrea D. Gonçalves,[§] Min Zhao,[#,∞] Gareth R. Williams,*[,†] Simon Gaisford,*[,†] and Duncan Q. M. Craig*[,†]

[†]UCL School of Pharmacy, University College London, 29-39 Brunswick Square, London, WC1N 1AX, U.K.

[§]DPDD Drug Delivery, GlaxoSmithKline R&D, Gunnels Wood Road, Stevenage, SG1 2NY, U.K.

[#]School of Pharmacy, Queen's University Belfast, 97 Lisburn Road, Belfast, BT9 7BL, U.K.

[∞]China Medical University-Queen's University Belfast Joint College (CQC), China Medical University, Shenyang 110000, China

* Corresponding authors. g.williams@ucl.ac.uk, +44 20 7753 5863 (G.R.W.); s.gaisford@ucl.ac.uk, +44 20 7 753 5868. (S.G.); duncan.craig@ucl.ac.uk, +44 20 7753 5819 (D.Q.M.C.).

Abstract

Amorphous solid dispersions (ASDs) of class II and IV Biopharmaceutics Classification System (BCS) drugs in water-miscible polymers are a well-recognized means of enhancing dissolution, while such dispersions in hydrophobic polymers form the basis of micro- and nanoparticulate technologies. However, drug recrystallization presents significant problems for product development and the mechanisms and pathways involved are poorly understood. Here we outline the use of combined differential scanning calorimetry (DSC)-synchrotron X-ray diffraction (XRD) to monitor the sequential appearance of polymorphs of olanzapine (OLZ) when dispersed in a range of polymers. In a recent study (*Cryst. Growth Des.* **2019**, 19, 2751−2757) we reported a new polymorph (form IV) of OLZ which crystallised from a spray dried dispersion of OLZ in polyvinylpyrrolidone. Here we extend our earlier study to explore OLZ dispersions in poly(lactide-co-glycolide) (PLGA), polylactide (PLA) and hydroxypropyl methyl cellulose acetate succinate (HPMCAS), with a view to identifying the sequence of form generation on heating each dispersion. While spray dried OLZ results in the formation of crystalline form I, the spray dried material with HPMCAS comprises an ASD, and forms I and IV are generated upon heating. PLGA and PLA result in a product which contains both amorphous OLZ and the dichloromethane solvate; upon heating the amorphous material converts to form IV and the solvate to forms I and II. Our data show that it is possible to quantitatively assess not only the polymorph generation sequence but also the relative proportions as a function of temperature. Of particular note is that the sequence of form generation is significantly more complex than may be indicated by DSC data alone, with coincident generation of different polymorphs and complex interconversions as the material is heated. We argue that this may have implications not only for mechanistic understanding of polymorph generation but also as an aid to identifying the range of polymorphic forms that may be produced by a single drug molecule.

Keywords: Pharmaceutical materials; polymorphism; amorphous solid dispersion; crystallization; differential scanning calorimetry; X-ray diffraction; synchrotron.

1. Introduction

The dissolution rate of an active pharmaceutical ingredient (API) may be highly dependent on physical form, and for Biopharmaceutics Classification System (BCS) Class II and IV drugs this may also have significant ramifications for bioavailability. Physical form may relate to particle size and shape, the crystal unit cell and composition (polymorphism, solvate formation) or amorphization; in addition, the dissolution performance may be influenced by the inclusion of other materials which can both control the form of the API and confer advantages to the dissolution profile. This strategy is increasingly widely used, particularly for drugs with poor water solubility, and is exemplified by amorphous solid dispersions (ASDs) whereby the drug is dispersed, typically (but not necessarily) on a molecular basis, in a water miscible polymer. Such an approach may lead to improved dissolution via a number of potential mechanisms, the one most commonly associated with molecular dispersions being the removal of the lattice enthalpy barrier to dissolution. There are a number of examples of clinical products based on ASDs such as Prograf™ (a tacrolimus formulation), Incivo® (telaprevir) and Intelence® (etravrine), as recently summarised by Lin *et al*.[1] In addition, drug dispersions in hydrophobic polymers such as polylactic/glycolic acid form the basis of many proprietary micro and nanoparticulate systems, and hence the understanding of drug dispersion in polymers is a matter of broad interest.

A major challenge is the possibility of physical instability; this is especially problematic for amorphous molecular dispersions which may recrystallize on storage, particularly at temperatures approaching or above the glass transition of the composite material. The propensity for this to occur will depend on the solubility of the drug in the polymer and the extent and nature of polymer/drug interactions, as well as the molecular mobility of the system. Both the propensity for recrystallization and the forms generated during this process are therefore highly important considerations. Taylor and co-workers have explored this phenomenon in detail, for instance looking at how the microstructure of ASDs affects crystallization and exploring the thermodynamics of polymer/drug mixing.[2,3] The same group devised a classification system to aid the prediction of drug crystallization behaviour.[4]

Here we study the recrystallization of olanzapine (OLZ), a low molecular weight (312 Da) heterocyclic antipsychotic drug with low aqueous solubility. ASDs of OLZ have been prepared in the past and shown to be able to accelerate dissolution rate, with the functional performance being dependent both on the polymer used and the extent of drug crystallinity in the formulations.[5] Four anhydrous polymorphic forms of OLZ have

been identified, as well as more than 60 solvates and hydrates.[6–9] These are virtually all based on dimeric building blocks. Recent work has developed methods to understand and quantify OLZ crystallization from ASDs,[10] but, owing in part to its complex polymorphism, understanding the phase transitions remains very challenging. Consequently, there is a paucity of information on the processes by which different polymorphs are generated as a function of temperature or time.

Simultaneous analysis with multiple techniques has been established as a promising strategy to obtain the information required to identify phase changes in ASDs. Differential scanning calorimetry (DSC) combined with FTIR, near-IR and Raman spectroscopy has been employed to this end.[11–15] However, while these spectroscopic techniques do provide insights into the physical form of the drug, X-ray diffraction (XRD) is a significantly more powerful structural approach. Previous work has been performed to combine DSC and XRD analysis by mounting heavily modified differential scanning calorimeters in synchrotron X-ray sources.[16–18] Unfortunately, the extensive modifications required in these experiments make them challenging to implement, and the datasets obtained are not directly comparable with standard lab DSC data.

To overcome this issue, we recently developed a new DSC-XRD analytical platform which required only minor modification to the DSC instrument.[19] By simply drilling two suitably placed holes in the exterior of the furnace on a standard lab instrument, we were able to mount a DSC on Beamline I12 of the Diamond Light Source and obtain XRD and DSC data simultaneously. This approach has led to enhanced understanding of phase transitions in glutaric acid and sulfathiazole,[19] carbamazepine and dihydrocarbamazapine,[20] and paracetamol.[21] Most recently, we employed the DSC-XRD platform with crystal structure prediction work and were able to identify and solve the structure of a new polymorph of OLZ which crystallised from an OLZ-polyvinylpyrrolidone ASD.[22] Unlike virtually all previous OLZ polymorphs and pseudopolymorphs, the new form (form IV) is not based on dimeric units, but rather has a very different molecular packing arrangement.

In this work, we build on our earlier study[22] to explore three further OLZ-polymer dispersions, with the aim of understanding better the influence of the polymer on the drug recrystallization process. ASDs were produced by spray drying and characterised both using DSC alone and by simultaneous DSC-XRD. In this manner we intended to develop an understanding of the relationship between ASD polymer composition and the sequential formation of different crystal forms. This area has thus far remained unexplored, yet has significant implications for our understanding of instability in ASDs and how this can be prevented. Such understanding also has profound implications for enhancing interpretation of DSC profiles and also, crucially, as an aid to screening for new polymorphic forms, an issue of huge importance to the pharmaceutical industry.

2. Methods

2.1 Preparation of Olanzapine-Polymer Dispersions

OLZ-polymer dispersions were prepared via spray drying using a Mini B-290 Spray Dryer (Buchi, Switzerland) connected to a B-295 inert loop (Buchi, Switzerland) to achieve a closed system. All processing involved organic feed solvents and was performed under an inert atmosphere (< 6% O_2). This was achieved by purging the closed system with nitrogen gas. An aspirator rate of 100% was used in all experiments. Three different polymers were used: poly(lactide-co-glycolide) (PLGA), polylactide (PLA) or hydroxypropyl methyl cellulose acetate succinate (HPMCAS). Dispersions with theoretical compositions of 70% w/w olanzapine and 30% w/w polymer were generated in order to guarantee crystallization over an experimentally feasible time period; OLZ was also spray dried alone. The polymer grades, feed solution properties and processing conditions used to prepare each dispersion are summarised in Table 1. The solution and process parameters were individually optimised for each system as a result of the different polymer properties (e.g. solubility and viscosity). Samples were analysed by lab DSC within 1-2 days of being synthesised, and were three weeks old at the time of synchrotron experiments.

Table 1 – The polymer grades, feed solution properties and spray drying parameters used in this work.

System	Polymer Grade and supplier	Feed Solution	Spray Drying Nozzle Type	Processing Parameters
OLZ-PLGA	Purac® PDLG 5002A (Corbion, Gorinchem, NL)	7% w/w olanzapine and 3% w/w PLGA in dichloromethane	Ultrasonic	Inlet temperature = 60 °C Ultrasonic power = 1.0 W Pump rate = 1.25 mL/min
OLZ -PLA	Purac® PDL 02A (Corbion, Gorinchem, NL)	7% w/w olanzapine and 3% w/w PLA in dichloromethane	Ultrasonic	Inlet temperature = 60 °C Ultrasonic power = 1.0 W Pump rate = 1.25 mL/min
OLZ-HPMCAS	AQOAT® AS-LF (Shin-Etzu Ltd., Tokyo, Japan)	0.7% w/w olanzapine and 0.3% w/w HPMCAS in acetone	Ultrasonic	Inlet temperature = 65 °C Ultrasonic power = 1.0 W Pump rate = 5 mL/min
OLZ	N/A (Myjoy Ltd, Kolkata, India)	7% w/w olanzapine in dichloromethane	Ultrasonic	Inlet temperature = 60 °C Ultrasonic power = 1.0 W Pump rate = 1.25 mL/min

2.2 DSC

DSC data collection was performed with a Discovery DSC (TA Instruments, USA) from 0 °C to 200 °C at a heating rate of 10 °C/min. The cell was purged with nitrogen at a rate of 50 mL/min in all experiments. The temperature and cell constant were both calibrated before use with an indium standard. Samples (3-5 mg) were weighed into standard aluminium pans and sealed with aluminium lids (TA Instruments, USA) that had

a pinhole punched into them. All experiments were undertaken in triplicate. DSC data were analysed with TA Universal Analysis (TA Instruments, USA) and were plotted within the same software.

2.3 DSC-XRD

A simultaneous DSC-XRD analytical platform based on that described by Clout *et al.* was employed to capture heat flow and diffraction data concurrently.[19] A modified Q20 differential scanning calorimeter (TA Instruments, USA) was mounted on Beamline I12 at the Diamond Light Source (UK). The calorimeter was aligned so that a monochromated X-ray beam (diameter = 0.5 mm; λ = 0.23306 Å) passed directly through the entry and exit holes in the DSC cell, allowing diffraction data to be collected on a Thales Pixium RF4343 detector positioned 1.9 m behind the sample. The calorimeter was calibrated for temperature using an indium standard before the experiment. The detector was calibrated using CeO_2. Ca. 30 mg of the olanzapine dispersions were loaded into a Tzero aluminum DSC pan (TA Instruments, USA) and the sample was heated at a rate of 10 °C min^{-1} from 50 °C to 200 °C, with a diffraction pattern collected every 6 seconds (1 °C of heating). The 2D XRD data collected were processed to 1D diffraction patterns using the DAWN Science Workbench software.[23] In brief, this involved azimuthal integration, normalization to beam current, and background subtraction. Structural refinement was performed using the Rietveld method in the TOPAS Academic software (V5) [24] and the results were plotted in Origin 2018.

3. Results

3.1 OLZ

When spray dried OLZ was analysed using DSC, a single endotherm with a peak at 194.3 °C was seen (Supplementary Information, Figure S1). This is consistent with the melting point of form I.[7] There are no crystallization events observed, demonstrating that OLZ crystallizes during spray drying, despite the rapid solvent evaporation in the process and the relatively high T_g (68 °C) of OLZ.

3.2 OLZ-HPMCAS

DSC data obtained on the OLZ-HPMCAS formulation are presented in Figure S2, and show a broad endotherm at ca. 60 °C which can reasonably be attributed to residual solvent loss, an exotherm at 123.2 °C and two endotherms at 174.7 °C and 190.1 °C; there is some evidence of a glass transition at ca. 80 °C although this is partially obscured by the solvent loss peak. A contour plot of the XRD data and DSC thermogram from simultaneous DSC-XRD analysis of the OLZ-HPMCAS dispersion is presented in Figure 1. The first-order crystallization and melting transitions appear consistent in both the XRD and heat flow data. It appears that the spray dried material was amorphous, given the lack of Bragg reflections in XRD.

A large crystallisation exotherm with an onset of 119 °C is seen in the DSC-XRD data (Figure 1), and is coincident with the appearance of reflections. Two subsequent melting peaks were observed at 181.3 °C and 194.1 °C, although these were not fully resolved on the DSC. Thus, the DSC data obtained from the simultaneous measurement corresponded well to the standalone DSC data reported in Figure S2; the small differences observed can be attributed to variations in the mass of sample used and the age of the ASDs. It is not clear from the DSC data alone whether a standard endotherm-exotherm-endotherm pattern indicative of a melt-recrystallisation-melt process exists. This also renders the identification of the polymorphs present via the peak temperature and the enthalpies associated with the events unreliable. Furthermore, the melting point lowering effects caused by the presence of the polymer provides further difficulty in reliable peak assignation. That said, it might intuitively be expected that the endotherm at 194 °C is due to the melting of form I (reported to be 195 °C),[7] and the endotherm at 180 °C from form II, which according to the literature melts at 184 °C.[25] However, the recently reported form IV of OLZ has a melting point of 189 °C,[22] close to the higher temperature event. Overall, therefore, considerable interpretative uncertainty remains when using the DSC data alone.

Additional insights into the crystallisation of OLZ in the HPMCAS dispersion were obtained from the XRD data. The contour plot confirmed that appreciable amounts of crystalline material began to appear at 119 °C, since all the reflections became visible at this temperature. Looking at the plot in detail, it appears that there are at least two different crystalline forms present in the system, given that some reflections continue to grow in intensity as the temperature increases (e.g. that at ca. 1.3°), while others grow and decline (e.g. at ca. 2.9°).

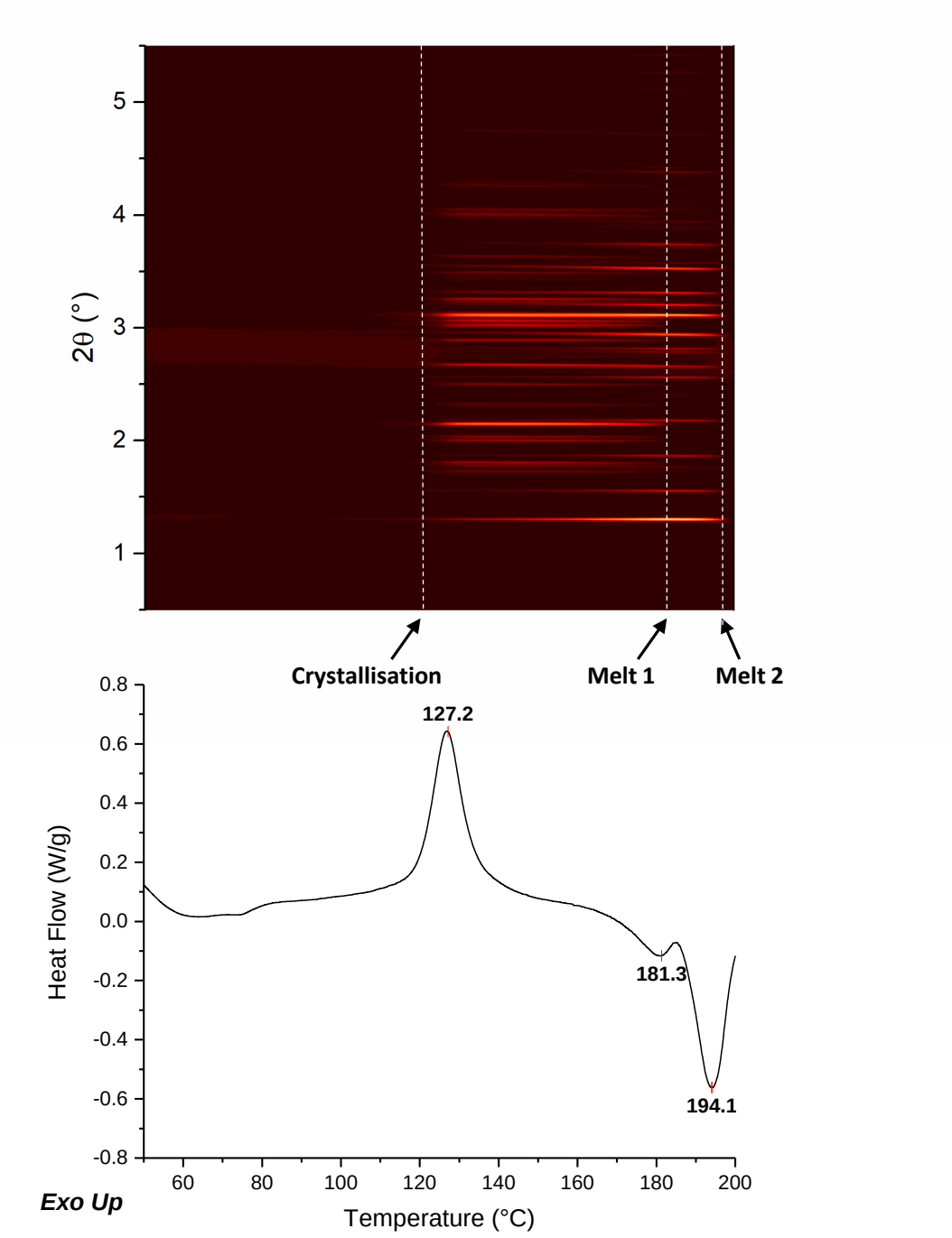

Figure 1 – Contour plot of XRD data (top) and DSC thermogram (bottom) for the OLZ-HMPCAS system

Individual XRD patterns recorded at increasing temperatures after the OLZ crystallisation event are displayed in Figure 2(a). Visual inspection of the XRD pattern recorded at 130 °C suggested a mixture of form IV and form I had crystallised. This was confirmed with simultaneous refinement of the models of both form IV and form I (Figure 2(b)) to the experimental data (R_{wp} = 6.74). This is only the second time that form IV OLZ has been observed, and it is notable that, as with the first report,[22] again this novel polymorph arises upon heating a polymer-based ASD. The presence of the polymer prevents determination of the amount of amorphous OLZ present (since the polymer also contributes to the amorphous part of the diffraction

pattern), but the relative content of each crystalline phase was calculated from the integrated area of each refined model (Figure 2). This analysis revealed that form IV was the main component present at 130 °C, forming 81.9% of the crystalline content (Table 2). The XRD pattern at 170 °C showed that the content of form I increased as a function of temperature, while the amount of form IV declined, and by 190 °C only form I remained Figure 2(c) and Table 2). The fate of form IV cannot be established conclusively, but we hypothesise that it converts to form I, given that the decline in form IV content begins well below its melting point.

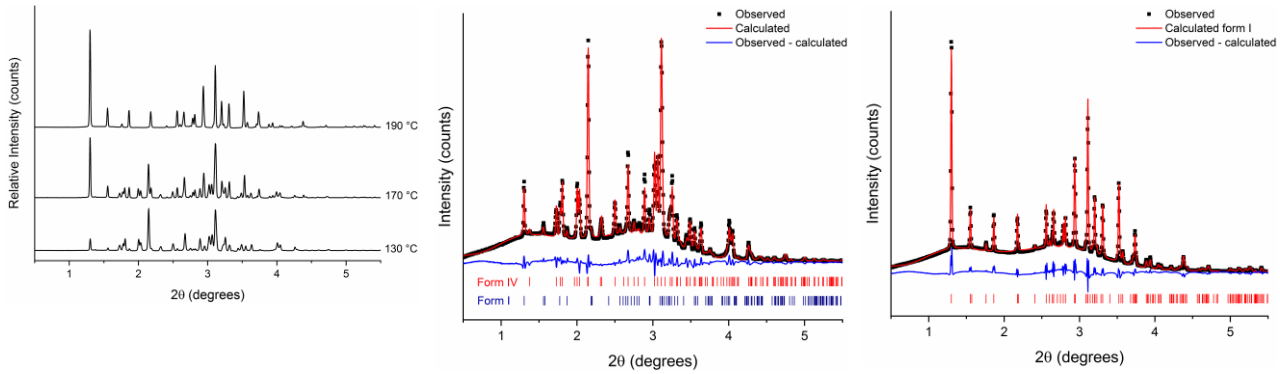

(a) **(b)** **(c)**

Figure 2 –XRD data for OLZ-HPMCAS, showing (a) patterns at selected temperatures after the onset of crystallisation and Rietveld refinements fitting OLZ forms I and IV to the data at (b) 130 and (c) 190 °C.

Table 2 – Refinement parameters for the XRD patterns recorded at 130 and 190 °C for OLZ-HPMCAS.

Temperature (°C)	**130**		**190**
Polymorph	OLZ IV	OLZ I	OLZ I
CSD ID	UNOGIN05	UNOGIN03	UNOGIN03
Relative content (%)[a]	81.9	18.1	100
Space group	*P 2₁/n*	*P 2₁/c*	*P 2₁/c*
***a* (Å)**	8.6166(4)	10.424(3)	10.448(2)
***b* (Å)**	15.460(12)	15.053(3)	15.168(2)
***c* (Å)**	12.522(1)	10.606(4)	10.630(3)
β (Å)	95.205(5)	100.87(5)	100.96(3)
***V* (Å³)**	1661.31(20)	1634.36(9)	1654.0(5)
R_{wp}	6.74		9.88

[a] Determined as phase fractions via integration of the diffraction patterns at each time point.

Batch refinements were then performed for the entire XRD dataset, which allowed the relative quantities of forms I and IV to be determined as a function of temperature (Figure 3).

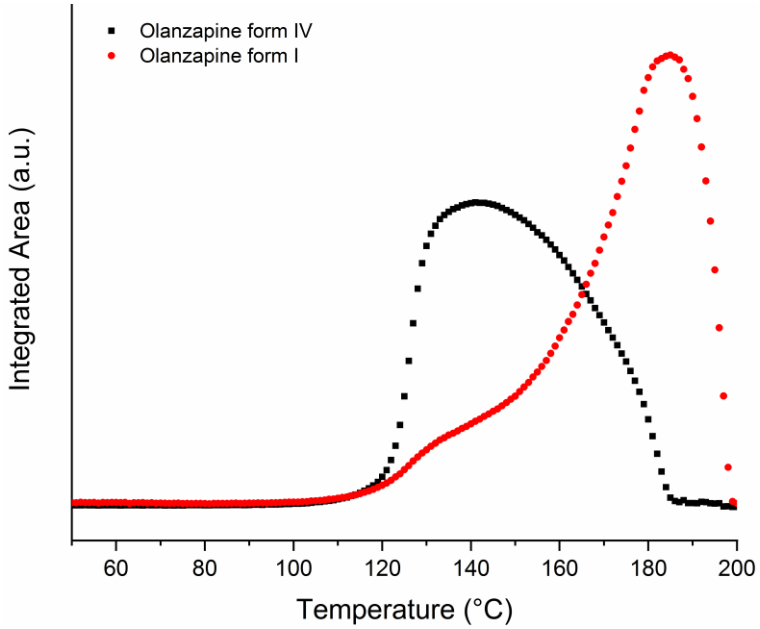

Figure 3 – Plot of the relative quantities of forms I and IV present in OLZ-HMPCAS as a function of temperature

To summarise, initially the dispersion was fully amorphous but as the temperature (and therefore molecular mobility) in the system increased, olanzapine crystallisation began at approximately 110 °C. Forms I and IV crystallised concurrently, although form IV crystallised more rapidly and was initially the predominant form. A further increase in temperature resulted in a reduction in the content of form IV and an increase in the content of form I, presumably due to the transition of olanzapine from form IV to form I. We hypothesise that as the temperature rises the increased molecular mobility permits the translational rearrangement of the OLZ moieties, such that they can convert from metastable form IV to stable form I. Finally, the melting of form I can be seen and the crystalline content reduces very sharply from 190 °C.

The melting point of form IV reported in the literature is 189 °C,[22] which is markedly higher than the completion of the IV → I transition. While some depression in melting point would be expected for a drug/polymer dispersion the fact that conversion to form I is complete a full 10 °C below the form IV melt, coupled with the lack of any recrystallization endotherm, indicates that the transition is most likely to be a solid/solid process. The lower melt at 180 °C in the DSC data presumably arises from the residual form IV melting and then not recrystallising: close inspection of the data in Figure 3 reveal that the rate of decline in the form IV intensity accelerates at this point.

Overall, therefore, what appears from the DSC data to be a simple event of recrystallization from the amorphous state into one form (initially anticipated to be form II) followed by a melt/recrystallization/melt into form I is in fact much more complex. The recrystallization event did not, as is commonly supposed, result in a single form recrystallizing but in fact represented a combination of two forms, form I and the newly discovered form IV, the latter undergoing a solid-solid transformation to form I on heating and the residual material simply melting at 180 °C without further recrystallization.

3.2 OLZ-PLA

The standalone DSC data (Figure S3) for the olanzapine/PLA dispersions indicated a T_g at approximately 53 ^oC (again coincident with a solvent loss peak), an exotherm at 102.4 ^oC and then two endothermic peaks at 178.0 ^oC and 189.1 ^oC. The results of the corresponding DSC-XRD analysis of the olanzapine-PLA dispersion are presented in Figure 4. Interestingly, the DSC data showed only a single endotherm while the presence of intense reflections in the contour plot at 50 °C showed that there was initial crystallinity present in the sample prior to heating. Additionally, two melts were clearly visible in the contour plot (with different reflections disappearing at different temperatures), whereas only one broad melt was observed in the thermogram. This is again of interest as it implies that the appearance of the single melting peak, albeit fairly broad and asymmetric, does not necessarily indicate the presence of a single polymorphic form.

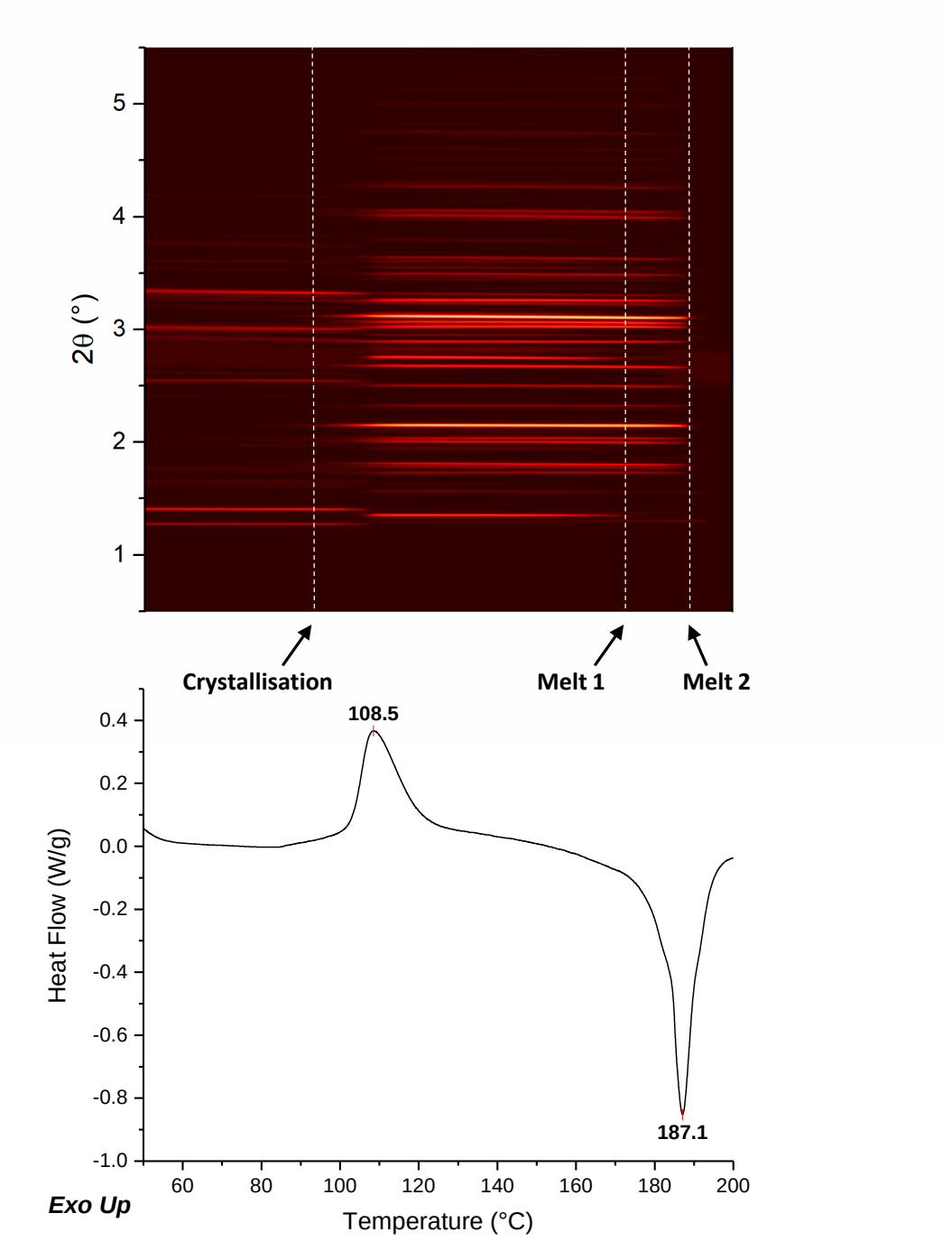

Figure 4 – Contour plot of XRD data (top) and DSC thermogram (bottom) for OLZ-PLA

Individual XRD patterns from three temperatures throughout the experiment are presented in Figure 5(a). The initial crystalline content in the dispersion at 50 °C appeared small, resulting in low intensity reflections, and the reflections at 1.27° and 1.40° did not match the characteristic reflections of any of the anhydrous forms. It was hypothesised that the dichloromethane (DCM) solvate of olanzapine had crystallised during or following spray drying, and that this was the initial crystallinity observed. This was proven correct through Rietveld refinement (Figure 5(b) and Table 3). The XRD patterns at low temperatures show a distinct halo background, typical of amorphous material (both OLZ and polymer) being present.

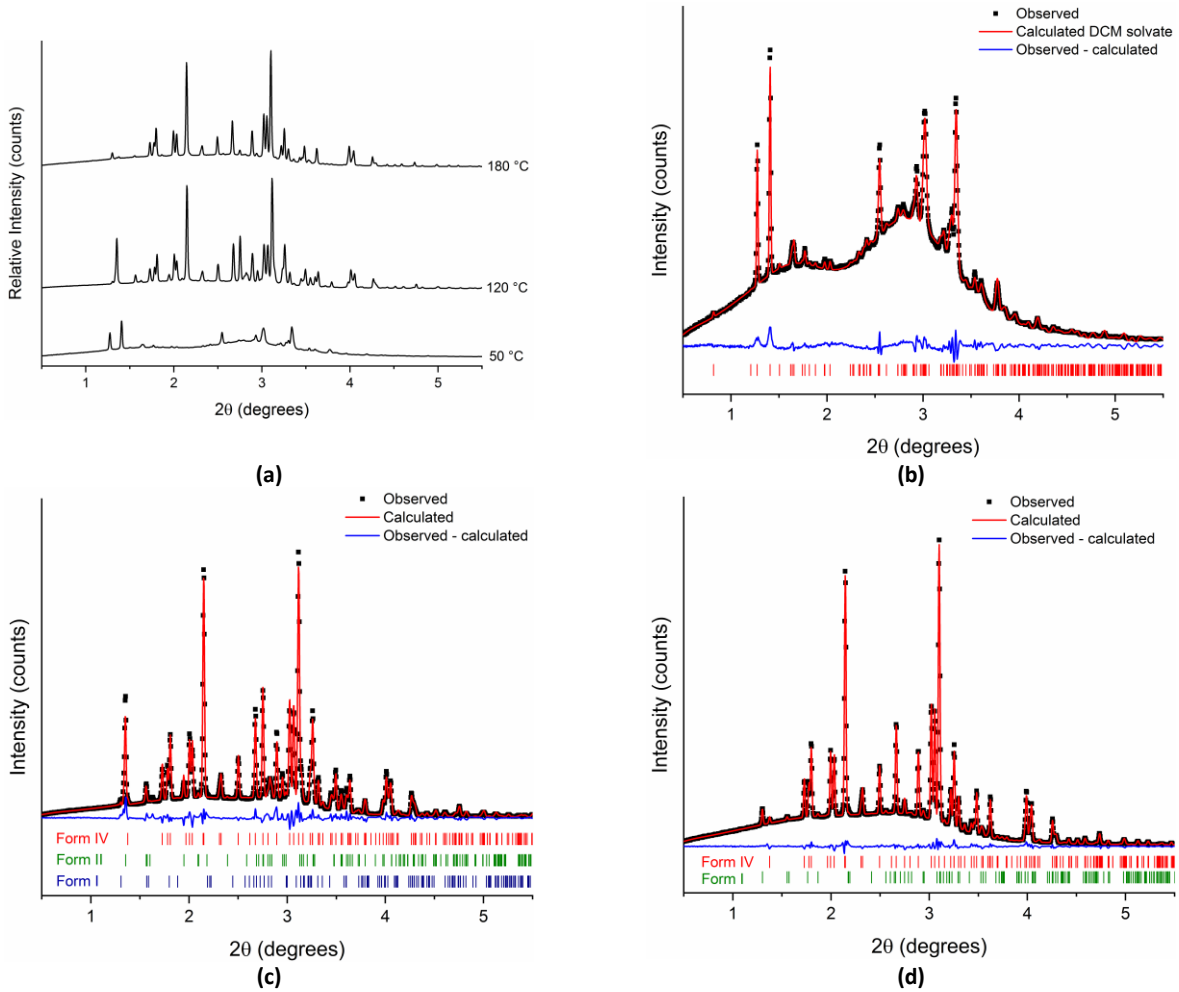

Figure 5 – XRD data for OLZ-PLA, showing (a) patterns at selected temperatures after the onset of crystallisation. Also given are Rietveld refinements fitting (b) the DCM solvate structure to the pattern at 50 °C, and OLZ forms I and IV to the data at (c) 120 and (d) 180 °C.

Following the crystallisation event, the characteristic reflections of the DCM solvate form disappear, as can be seen in the XRD pattern at 120 °C (Figure 5(a)). Rietveld refinement (Figure 5(c)) revealed that after recrystallization a mixture of OLZ forms I, II and IV was present. The results of the structural refinements at 120 °C again show that form IV was the predominant phase following crystallisation (65.2% of the crystalline content), followed by forms II and I respectively (Table 3). When the dispersion was heated further form II melted,[25] leaving a mixture of form IV (76.7%) and form I (23.3%) at 180 °C (see refinement in Figure 5(d)). In the PLA dispersion there was not a significant transition of form IV to form I upon heating (as was observed in the OLZ-HPMCAS system), despite form I seeds being present. Due to the low content of form I in the dispersion, and small difference in T_m between forms I and IV, the melt of form I cannot be easily observed in the contour plot (Figure 4), although the appearance and disappearance of a faint reflection at 1.3° can be seen close to the second melt.

Table 3 – Refinement parameters for the XRD patterns recorded at 50, 120 and 180 °C for the OLZ-PLA dispersion.

Temperature (°C)	**50**	**120**			**180**	
Polymorph	DCM solvate	OLZ I	OLZ II	OLZ IV	OLZ I	OLZ IV
CSD number	WEXQAS01	UNOGIN03	UNOGIN02	UNOGIN05	UNOGIN03	UNOGIN05
Relative content (%)[a]	100	14.6	20.2	65.2	23.3	76.7
Space group	*P -1*	*P $2_1/c$*	*P $2_1/c$*	*P $2_1/n$*	*P $2_1/c$*	*P $2_1/n$*
***a* (Å)**	9.7643(4)	10.14(2)	9.942(1)	8.605(3)	10.37(1)	8.649(2)
***b* (Å)**	11.615(2)	15.21(3)	16.668(2)	15.453(1)	15.10(2)	15.453(8)
***c* (Å)**	16.989(2)	10.71(5)	10.029(2)	12.512(8)	10.54(3)	12.542(7)
α (Å)	103.17(1)	90	90	90	90	90
β (Å)	97.07(1)	100.0(6)	97.66(2)	95.190(4)	100.3(4)	95.402(3)
γ (Å)	99.74(2)	90	90	90	90	90
***V* (Å^3)**	1822.8(3)	1628(9)	1647.2(3)	1657.1(2)	1625(6)	1669.1(1)
R_{wp}	3.87		8.46		5.99	

[a] Determined as phase fractions via integration of the diffraction patterns at each time point.

The relative quantities of the crystalline phases present were quantified and plotted as a function of temperature (Figure 6). The loss of the DCM solvate phase correlated very well with the concurrent appearance of forms I and II, which occurred in the temperature range of 90 to 110 °C. Given that the DCM solvate and forms I and II of OLZ all share the same dimeric building block, it is hypothesised that the solvate converts to form I and II via desolvation of the initial lattice and then subsequent molecular rearrangements to yield the anhydrous forms. This idea is borne out by the plot in Figure 6: the integrated areas for form I + II after conversion is complete match closely the initial area of the DCM solvate. Form IV is observed to start crystallising before the DSC exotherm, with form IV reflections first appearing at 80 °C. Form IV then proceeds to become the predominant crystalline form in the dispersion until its melting is complete at 190 °C. The quantities of forms I and II remained relatively low throughout the experiment, and these materials can be seen to melt at 175 °C and 195 °C respectively. The content of form I did start to increase as form IV melted, but there was insufficient time for a significant melt/recrystallization to occur because form I melted soon afterwards. From these data, it appears that after spray drying some of the OLZ has crystallized into the DCM solvate while some remains amorphous. The former converts to OLZ I and II upon heating, while the latter converts to forms I, II and IV.

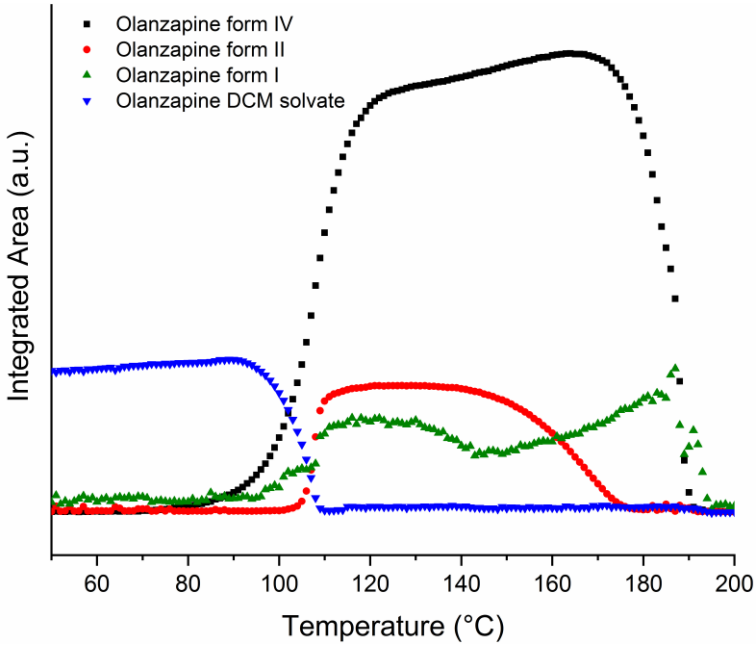

Figure 6 – Plot of the relative quantities of the crystalline forms present as a function of temperature in the OLZ-PLA dispersion

3.3 OLZ-PLGA

The DSC data on OLZ-PLGA (Figure S4) show a T_g at 46.4 °C, an exotherm at 105.8 °C and endotherms at 177.8 °C and 188.5 °C, with the former being of clearly greater preponderance. The results of DSC-XRD analysis are summarised in Figure 7. Again, there were discrepancies between the two sets of DSC data (with the combined technique showing a single broad endothermic peak at 187.1 °C) which we ascribe to slight differences in storage times prior to measurement and/or sample sizes, in turn resulting in differences in the degree of initial crystallinity and/or nucleation. The preponderance of the lowing melting peak seen with the standalone DSC was not apparent with the combined technique.

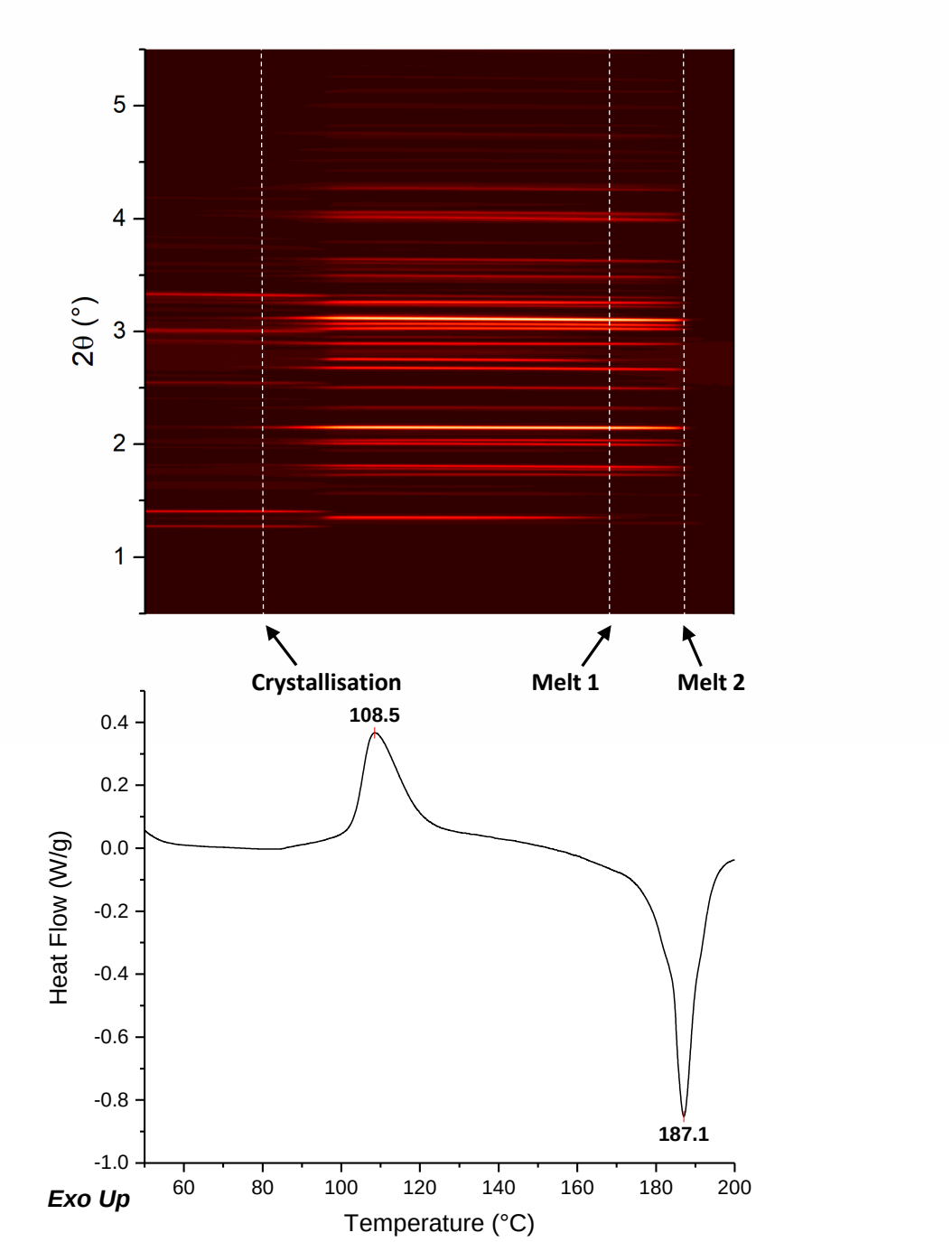

Figure 7 – Contour plot of XRD data (top) and DSC thermogram (bottom) for OLZ-PLGA

Inspection of individual XRD patterns (Figure 8) again confirmed that the DCM solvate was present, due to the characteristic reflections at 1.27° and 1.40°. At 120 °C, following the crystallisation event in DSC, the reflections of form II are evident. At 180 °C the characteristic reflection of form I at 1.30° becomes clear following the melting of form II.

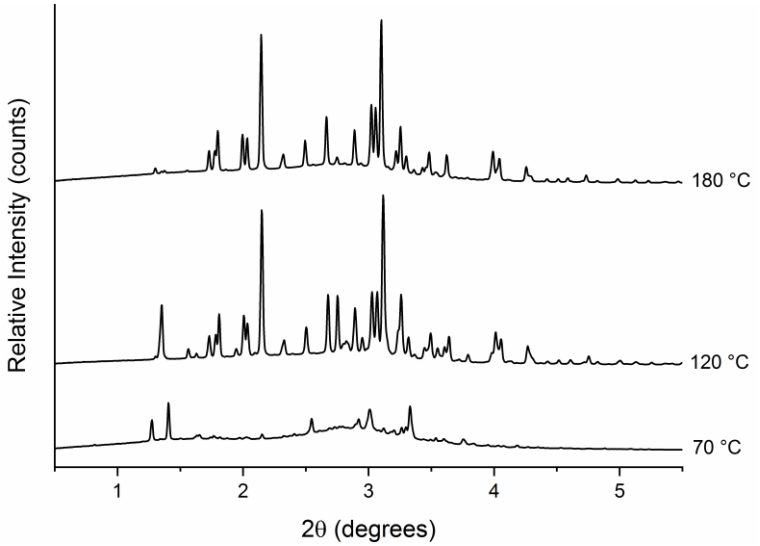

Figure 8 – Individual XRD diffraction patterns of the OLZ-PLGA dispersion recorded at 70 °C, 120 °C and 180 °C. Reflections marked in at 120 °C are characteristic of form II, and that at 180 °C is characteristic of form I.

Batch refinements of the entire XRD dataset were performed and the relative quantities of each phase as a function of temperature are presented in Figure 9. This plot is almost identical to Figure 6, showing that the phase transitions in the PLA and PLGA dispersions were the same. Again, it appears that OLZ IV crystallizes from amorphous drug present in the spray dried particles, while the DCM hydrate converts to form I and II.

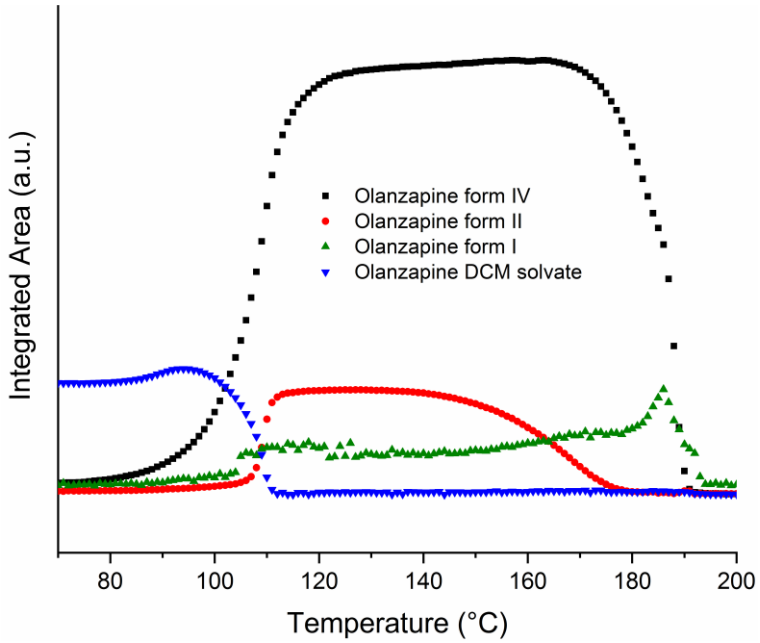

Figure 9 – Plot of the relative quantities of the crystalline forms present as a function of temperature in the OLZ-PLGA dispersion

4. Discussion

The data presented above and our previous study[22] clearly show that crystallising OLZ from different polymer dispersions affects the polymorphic forms obtained. This is summarised in Table 4.

Table 4 – Summary of the olanzapine polymorphs that crystallised in each polymer dispersion

Dispersion	Form I	Form II	Form III	Form IV	DCM solvate
PVP[a]	-	-	-	✓*	-
HPMCAS	✓	-	-	✓*	-
PLA	✓	✓	-	✓*	✓
PLGA	✓	✓	-	✓*	✓

✓signifies that the form was observed in the dispersion and ✓ signifies that this was the predominant form following crystallisation.*
[a] Data collected in a previous study and reported in reference [22].

The most notable trends in the results were that: (1) the recently discovered form IV was the predominant polymorph that crystallised in all of the dispersions; and (2) the same combination of forms crystallised in the PLA and PLGA systems (when the polymer properties including viscosity were very similar, albeit with greater hydrophobicity for the former), whereas different combinations crystallised in the PVP and HPMCAS systems (when the polymer properties were changed significantly). The implications of these observations are that some property present in all of the dispersions is favouring the crystallisation of olanzapine form IV, and that the specific polymer properties determined whether this would crystallise as a pure or mixed phase. The solvent used for spray drying also seems important: the HPMCAS material was prepared from acetone, and an entirely amorphous dispersion formed. The PLA and PLGA formulations were made from a DCM solution, resulting in some of the material crystallizing into the DCM solvate in the drying process. However, the previously reported PVP formulation was also prepared from DCM,[22] and here spray drying results in an amorphous material. In all four cases, it appears that OLZ form IV crystallizes from amorphous OLZ in the dispersion, with form I also being generated from the amorphous OLZ material in the case of HPMCAS and I and II for PLA and PLGA. Where the DCM solvate forms, this is seen to convert to forms I and II upon heating.

Ostwald's rule of stages posits that metastable forms will crystallise first because they are closest in energy to the amorphous form and this will be followed by recrystallisation to the thermodynamically stable phase.[26] Although not a universal rule, it has been shown to be true for many compounds,[27] and the work presented here shows that it is applicable to these systems since the known stable form of olanzapine, form I, was not the first polymorph to crystallise in any of the dispersions. The increased viscosity of the amorphous phase caused by the polymer could be kinetically trapping metastable forms of OLZ (II and IV), as was previously observed in dispersions of paracetamol where the viscosity of different HPMC grades affected the amount of metastable polymorphs II and III that crystallised in each dispersion.[28] However, this mechanism alone does not explain why OLZ form II has been the product of numerous crystallisation experiments, yet form IV has never been observed to precipitate from solution despite it having a lower calculated lattice energy and higher T_m.[22]

Until the recent discovery of OLZ form IV by heating an OLZ-PVP ASD,[22] virtually all known anhydrous forms and solvates of OLZ were based on the SC_0 dimer (a centrosymmetric supramolecular construct; see Figure 10), proposed to be because of self-association of OLZ molecules into these dimers in the solution state.[7] As a result of this, most of the molecules involved in short length-scale aggregation prior to nucleation are present in the dimer form, resulting in the crystallisation of forms exclusively containing this structural motif. Supporting evidence for this theory is given by the example of tetrolic acid, where solutions rich in dimers of tetrolic acid crystallised to the α polymorph (in which dimers are the core structural unit), and solutions in which dimer formation was disrupted gave the catemeric β form.[29] A degree of molecular arrangement has also been observed in an amorphous melt-quenched phase of carbamazepine.[30]

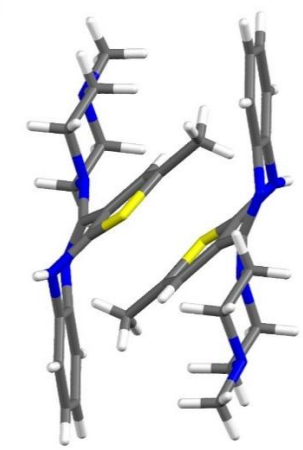

Figure 10 – Two olanzapine molecules arranged in the SC_0 packing motif thought to be the essential building block of crystalline forms of olanzapine (drawn in Mercury software)

All of the polymers studied are capable of forming hydrogen bonds with OLZ molecules. These specific directional interactions are stronger than the weak C–H···π contacts that stabilise olanzapine dimers and therefore it is reasonable to speculate that OLZ will interact with the polymers through H-bonding rather than forming dimers. OLZ molecules that begin associating into aggregates prior to nucleation in the polymer dispersions may therefore be able to start organising into alternative low energy structures, such as the structure of form IV. The molecules in OLZ form IV interact through hydrogen bonding (Figure 11) which could be promoted by chemical templating by the polymers if OLZ molecules are already interacting with the polymer in this way. The presence of hydrogen bonds has not been proven in these dispersions, but these interactions have been observed in many other drug-polymer systems and it is reasonable to speculate that they will occur here.[31–33]

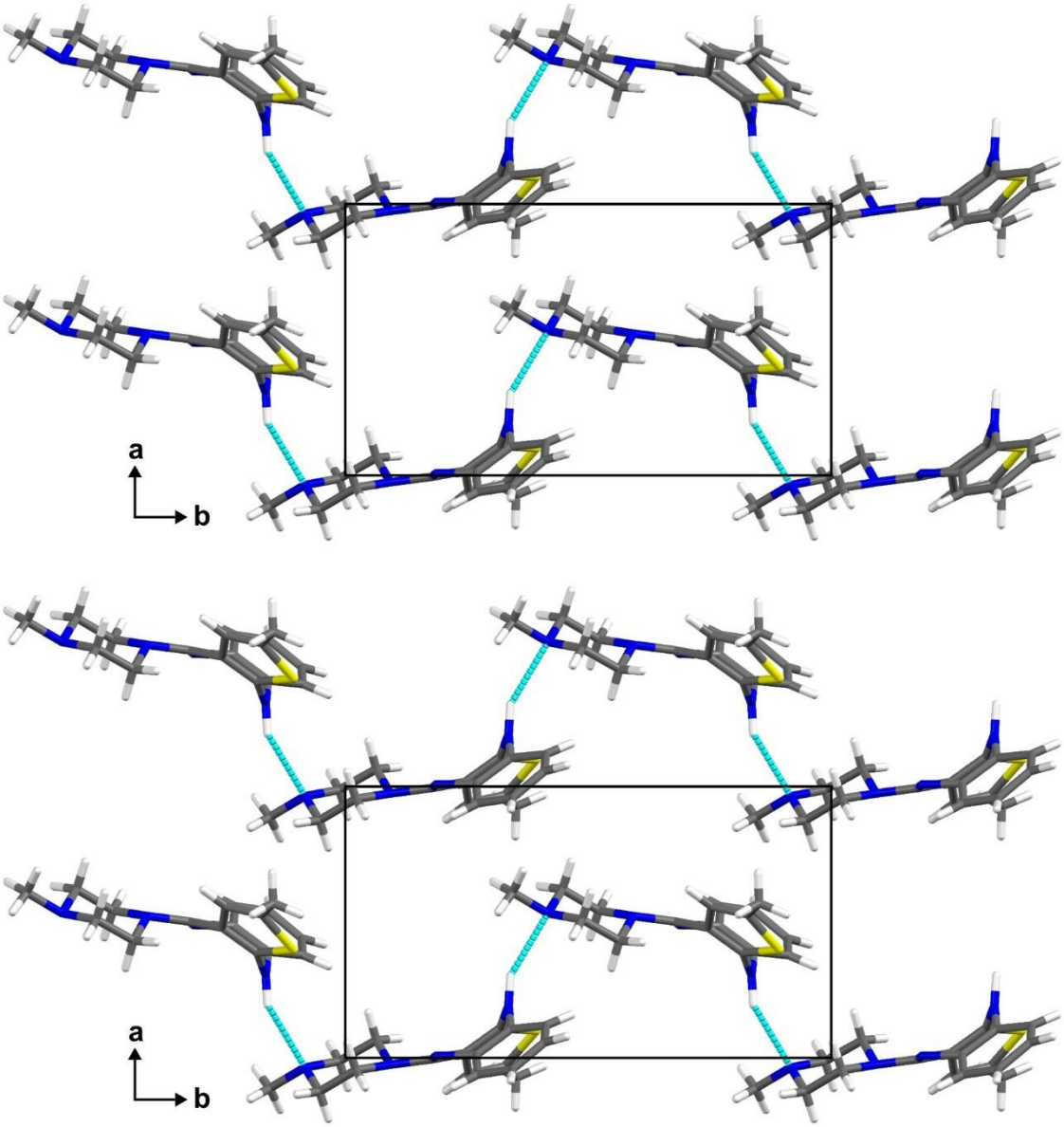

Figure 11 – Hydrogen bonding between olanzapine molecules in olanzapine form IV and the unit cell (drawn in Mercury software)

OLZ has been crystallised from many solvents with which it is capable of forming hydrogen bonds (e.g. water, ethanol and acetone), yet form IV was not the product of any of these crystallisations.[7] This suggests that crystallising from the super-cooled liquid state was also critical for the crystallisation of form IV, presumably due to the higher viscosity of this state relative to a solution. In a highly viscous polymer dispersion the level of mobility of the OLZ molecules will be significantly lower, therefore there will be limited opportunity for the molecules to re-orientate themselves into dimers through Brownian motion. In solution, however, the mobility of the molecules will be many orders of magnitude greater and therefore the molecules will form dimers rapidly. OLZ dimerization helps the drug to mask its hydrophobicity from the water and is themodynamically favourable compared to hydrogen bonding with water molecules. The evidence available

suggests that it is a combination of both the physical and chemical properties of the polymer dispersions that promoted the crystallisation of OLZ form IV in each of the systems.

Polymers have been shown to affect the crystallisation of a number of polymorphic drugs in the literature. For example, insoluble polymer heteronuclei were found to direct crystallisation and promote the formation of certain polymorphs in solution crystallisations,[34,35] based on the accessibility of polymer functional groups at the interface affecting intermolecular interactions and directing nucleation of a specific form.[36] Polymer surfaces have also been shown to direct crystallisation of the metastable α indomethacin polymorph from the amorphous melt by chemical templating,[37] and the highly unstable form III of paracetamol preferentially crystallises from the amorphous melt in the presence of β-1,4-saccharides (lactose and HPMC).[21] In the latter case, the sugar plays an active role in stabilising the highly metastable paracetamol form via intermolecular interactions.

Although form IV was the predominant polymorph observed in all three dispersions reported here (and was the only form noted in our previous study using PVP as the polymer carrier[22]), form I also concurrently crystallised in the HPMCAS system, and forms I and II were present in the PLA and PLGA systems. The crystallisation behaviour was nearly identical in the PLA and PLGA systems. The latter is to be expected, as chemically PLA and PLGA are similar, and the grades used in this work have similar viscosities. The DCM solvate of olanzapine was present in the PLA and PLGA dispersions, and must have formed during or after the spray drying process. The DCM solvate contains the SC_0 dimer motif and desolvation of this structure previously resulted in mixtures of forms I and II.[7] Analysis of the batch refinement data showed that the loss of the DCM solvate phase correlated well with the appearance of forms I and II (Figures 6 and 9). Conversely, form IV begins crystallising before the loss of the DCM solvate, suggesting that two separate events are occurring: (1) crystallisation of form IV from the amorphous molecules of olanzapine; and (2) desolvation of the DCM solvate resulting in the formation of a mixture of the structurally similar forms I and II via a solid-solid transition. This analysis suggests that the presence of forms I and II in the PLA and PLGA dispersions were not solely due to the polymer properties, but could be a result of the presence of the DCM solvate after the spray drying process.

In the HPMCAS system, form I concurrently crystallises with form IV, but this does not occur in the previously reported PVP system.[22] The reason for the different behaviour of these two systems is not clear. The presence of multiple forms may be due to the inherent ability of each polymer to promote the formation of form IV (i.e. the structure of HPMCAS is less successful at disrupting the formation of dimers, therefore some of the thermodynamically stable phase also crystallises).

5. Conclusions

The crystallization of olanzapine (OLZ) from amorphous dispersions prepared in poly(lactide-co-glycolide) (PLGA), polylactide (PLA) and hydroxypropyl methyl cellulose acetate succinate (HPMCAS) was explored in this work. When OLZ is spray dried the product comprises crystalline form I. Using HPMCAS as the polymer carrier, the spray dried material comprises an amorphous SD, and forms I and IV of OLZ are generated upon heating. PLGA and PLA result in a product which contains both amorphous OLZ and the dichloromethane solvate. Form IV OLZ is based on H-bonded catamers, while all other known polymorphs and solvates are built up from SC_0 dimer units. This is only the second time that form IV of OLZ has been reported, with the previous report also using a drug-polymer dispersion. The use of polymers as solvents for active pharmaceutical ingredients is therefore a promising route to identify new polymorphs. It is also clear that both the polymer and the solvent used for spray drying have a profound effect on the crystallization behaviour of the dispersion. It is hypothesised that this arises because of both the viscosity of the polymer and its ability to form intermolecular interactions with the incorporated drug molecules.

6. Acknowledgements

The authors would like to thank the Centre for Doctoral Training in Advanced Therapeutics and Nanomedicine and the EPSRC for funding (EP/L01646X). We further thank the Diamond Light Source for the provision of beamtime (EE17450), and Dr Oxana Magdysyuk for assistance during DSC−XRD experiments.

7. Supporting Information

Supporting Information is available free of charge on the ACS Publications website at DOI. DSC data for spray dried OLZ, OLZ-HPMCAS, OLZ-PLA, and OLZ-PLGA.

8. References

1. Lin, X., Hu, Y., Liu, L., Su, L., Li, N., Yu, J., Tang, B. & Yang, Z. Physical Stability of Amorphous Solid Dispersions: a Physicochemical Perspective with Thermodynamic, Kinetic and Environmental Aspects. *Pharm. Res.* **35,** (2018).

2. Li, N. & Taylor, L. S. Microstructure Formation for Improved Dissolution Performance of Lopinavir Amorphous Solid Dispersions. *Mol. Pharm.* (2019). doi:10.1021/acs.molpharmaceut.9b00117

3. Marsac, P. J., Li, T. & Taylor, L. S. Estimation of Drug–Polymer Miscibility and Solubility in Amorphous Solid Dispersions Using Experimentally Determined Interaction Parameters. *Pharm. Res.* **26,** 139–151 (2009).

4. Baird, J. A., van Eerdenbrugh, B. & Taylor, L. S. A Classificaion System to Assess the Crystallization Tendency of Organic Molecules from Undercooled Melts. *J. Pharm. Sci.* **99,** 3787–3806 (2010).

5. Pina, M. F., Zhao, M., Pinto, J. F., Sousa, J. J. & Craig, D. Q. M. The Influence of Drug Physical State on the Dissolution Enhancement of Solid Dispersions Prepared Via Hot-Melt Extrusion: A Case Study Using Olanzapine. *J. Pharm. Sci.* **103,** 1214–1223 (2014).

6. Reutzel-Edens, S. M., Bush, J. K., Magee, P. A., Stephenson, G. A. & Byrn, S. R. Anhydrates and Hydrates of Olanzapine: Crystallization, Solid-State Characterization, and Structural Relationships. *Cryst. Growth Des.* **3,** 897–907 (2003).

7. Bhardwaj, R. M., Price, L. S., Price, S. L., Reutzel-Edens, S. M., Miller, G. J., Oswald, I. D. H., Johnston, B. F. & Florence, A. J. Exploring the Experimental and Computed Crystal Energy Landscape of Olanzapine. *Cryst. Growth Des.* **13,** 1602–1617 (2013).

8. Sun, Y., Tilbury, C. J., Reutzel-edens, S. M., Bhardwaj, R. M., Li, J. & Doherty, M. F. Modeling Olanzapine Solution Growth Morphologies. *Cryst. Growth Des.* **18,** 905–911 (2018).

9. Bhardwaj, R. M., Reutzel-Edens, S. M., Johnston, B. F. & Florence, A. J. A random forest model for predicting crystal packing of olanzapine solvates. *CrystEngComm* **20,** 3947–3950 (2018).

10. Askin, S., Zhao, M., Gonçalves, A. D., Gaisford, S. & Craig, D. Q. M. The Development of Quasi-isothermal Calorimetry for the Measurement of Drug–Polymer Miscibility and Crystallization Kinetics: Olanzapine-Loaded PLGA Microparticles. *Mol. Pharm.* **15,** 3332–3342 (2018).

11. Mirabella, F. M. Simultaneous Differential Scanning Calorimetry (DSC) and Infrared Spectroscopy Using an Infrared Microsampling Accessory (IRMA) and FT-IR. *Appl. Spectrosc.* **40,** 417–420 (1986).

12. Pandita, S. D., Wang, L., Mahendran, R. S., Machavaram, V. R., Irfan, M. S., Harris, D. & Fernando, G. F. Simultaneous DSC-FTIR spectroscopy: Comparison of cross-linking kinetics of an epoxy/amine resin system. *Thermochim. Acta* **543,** 9–17 (2012).

13. Buanz, A. B. M., Telford, R., Scowen, I. J. & Gaisford, S. Rapid preparation of pharmaceutical co-crystals with thermal ink-jet printing. *CrystEngComm* **15,** 1031–1035 (2013).

14. Ali, H. R. H., Edwards, H. G. M. & Scowen, I. J. Insight into thermally induced solid-state polymorphic transformation of sulfathiazole using simultaneous in situ raman spectroscopy and differential scanning calorimetry. *J. Raman Spectrosc.* **40,** 887–892 (2009).

15. Sprunt, J. C., Jayasooriya, U. A. & Wilson, R. H. A simultaneous FT-Raman-DSC (SRD) study of polymorphism in sn-1,3-distearoyl-2-oleoylglycerol (SOS). *Phys. Chem. Chem. Phys.* **2,** 4299–4305 (2000).

16. Gilbert, E. P., Nelson, A., Sutton, D., Terrill, N., Martin, C., Lal, J. & Lang, E. Phase separation in the organic solid state: The influence of quenching protocol in unstable n-alkane blends. *Mol. Cryst. Liq. Cryst.* **440,** 93–105 (2005).

17. Bayés-García, L., Calvet, T., Àngel Cuevas-Diarte, M., Ueno, S. & Sato, K. In situ observation of transformation pathways of polymorphic forms of 1,3-dipalmitoyl-2-oleoyl glycerol (POP) examined with synchrotron radiation X-ray diffraction and DSC. *CrystEngComm* **15,** 303–314 (2013).

18. Brubach, J. B., Jannin, V., Mahler, B., Bourgaux, C., Lessieur, P., Roy, P. & Ollivon, M. Structural and thermal characterization of glyceryl behenate by X-ray diffraction coupled to differential calorimetry and infrared spectroscopy. *Int. J. Pharm.* **336,** 248–256 (2007).

19. Clout, A., Buanz, A. B. M., Prior, T. J., Reinhard, C., Wu, Y., O'Hare, D., Williams, G. R. & Gaisford, S. Simultaneous Differential Scanning Calorimetry-Synchrotron X-ray Powder Diffraction: A Powerful Technique for Physical Form Characterization in Pharmaceutical Materials. *Anal. Chem.* **88,** 10111–10117 (2016).

20. Clout, A. E., Buanz, A. B. M., Gaisford, S. & Williams, G. R. Polymorphic Phase Transitions in Carbamazepine and 10,11-Dihydrocarbamazepine. *Chem. - A Eur. J.* (2018). doi:10.1002/chem.201802368

21. Telford, R., Seaton, C. C., Clout, A., Buanz, A., Gaisford, S., Williams, G. R., Prior, T. J., Okoye, C. H., Munshi, T. & Scowen, I. J. Stabilisation of metastable polymorphs: the case of paracetamol form III. *Chem. Commun.* **52,** 12028–12031 (2016).

22. Askin, S., Cockcroft, J. K., Price, L. S., Gonçalves, A. D., Zhao, M., Tocher, D. A., Williams, G. R., Gaisford, S. & Craig, D. Q. M. Olanzapine Form IV: Discovery of a New Polymorphic Form Enabled by Computed Crystal Energy Landscapes. *Cryst. Growth Des.* (2019). doi:10.1021/acs.cgd.8b01881

23. Basham, M., Filik, J., Wharmby, M. T., Chang, P. C. Y., El Kassaby, B., Gerring, M., Aishima, J., Levik, K., Pulford, B. C. A., Sikharulidze, I., Sneddon, D., Webber, M., Dhesi, S. S., Maccherozzi, F., Svensson, O., Brockhauser, S., Náray, G. & Ashton, A. W. Data Analysis WorkbeNch (DAWN). *J. Synchrotron Radiat.* **22,** 853–858 (2015).

24. Coelho, A. A., Evans, J., Evans, I., Kern, A. & Parsons, S. The TOPAS symbolic computation system. *Powder Diffr.* **26,** S22–S25 (2011).

25. Cavallari, C. Thermal Study of Anhydrous and Hydrated Forms of Olanzapine. *Pharm. Anal. Acta* **4,** (2013).

26. Ostwald, W. Studien über die Bildung und Umwandlung fester Körper. 1. Abhandlung: Übersättigung und Überkaltung. *Zeitschrift für Phys. Chemie* **22,** 289–330 (1897).

27. Nývlt, J. The Ostwald Rule of Stages. *Cryst. Res. Technol.* **30,** 443–449 (1995).

28. Gaisford, S., Buanz, A. B. M. & Jethwa, N. Characterisation of paracetamol form III with rapid-heating DSC. *J. Pharm. Biomed. Anal.* **53,** 366–370 (2010).

29. Parveen, S., Davey, R. J., Dent, G. & Pritchard, R. G. Linking solution chemistry to crystal nucleation: The case of tetrolic acid. *Chem. Commun.* 1531–1533 (2005). doi:10.1039/b418603f

30. Billinge, S. J. L., Dykhne, T., Juhás, P., Boin, E., Taylor, R., Florence, A. J. & Shankland, K. Characterisation of amorphous and nanocrystalline molecular materials by total scattering. *CrystEngComm* **12,** 1366–1368 (2010).

31. Matsumoto, T. & Zografi, G. Physical Properties of Solid Molecular Dispersions of Indomethacin with Poly(vinylpyrrolidone) and Poly(vinylpyrrolidone-co-vinyl-acetate) in Relation to Indomethacin Crystallization. *Pharm. Res.* **16,** 1722–1728 (1999).

32. Gupta, P. & Bansal, A. K. Molecular interactions in celecoxib-PVP-meglumine amorphous system. *J. Pharm. Pharmacol.* **57,** 303–310 (2005).

33. Marsac, P. J., Shamblin, S. L. & Taylor, L. S. Theoretical and practical approaches for prediction of drug-polymer miscibility and solubility. *Pharm. Res.* **23,** 2417–2426 (2006).

34. Lang, M., Grzesiak, A. L. & Matzger, A. J. The use of polymer heteronuclei for crystalline polymorph selection. *J. Am. Chem. Soc.* **124,** 14834–14835 (2002).

35. Price, C. P., Grzesiak, A. L. & Matzger, A. J. Crystalline polymorph selection and discovery with polymer heteronuclei. *J. Am. Chem. Soc.* **127,** 5512–5517 (2005).

36. Lopez-Mejías, V., Knight, J. L., Brooks, C. L. & Matzger, A. J. On the mechanism of crystalline polymorph selection by polymer heteronuclei. *Langmuir* **27,** 7575–7579 (2011).

37. McKellar, S. C., Urquhart, A. J., Lamprou, D. A. & Florence, A. J. Polymer templating of supercooled indomethacin for polymorph selection. *ACS Comb. Sci.* **14,** 155–159 (2012).

For Table of Contents use only

A Simultaneous Differential Scanning Calorimetry – X-Ray Diffraction Study of Olanzapine Crystallisation from Amorphous Solid Dispersions

Sean Askin,[†] Andrea D. Gonçalves,[§] Min Zhao,[#,∞] Gareth R. Williams,*[,†] Simon Gaisford,*[,†] and Duncan Q. M. Craig*[,†]

[†]UCL School of Pharmacy, University College London, 29-39 Brunswick Square, London, WC1N 1AX, U.K.

[§]DPDD Drug Delivery, GlaxoSmithKline R&D, Gunnels Wood Road, Stevenage, SG1 2NY, U.K.

[#]School of Pharmacy, Queen's University Belfast, 97 Lisburn Road, Belfast, BT9 7BL, U.K.

[∞]China Medical University-Queen's University Belfast Joint College (CQC), China Medical University, Shenyang 110000, China

* Corresponding authors. g.williams@ucl.ac.uk, +44 20 7753 5863 (G.R.W.); s.gaisford@ucl.ac.uk, +44 20 7 753 5868. (S.G.); duncan.craig@ucl.ac.uk, +44 20 7753 5819 (D.Q.M.C.).